Signatures of a Universal Spectrum for Nonlinear Variability in Daily Columnar Total Ozone Content

A.M.Selvam and *M.Radhamani*
Indian Institute of Tropical Meteorology, Pune 411008, India
Received December 6, 1992; revised February 15, 1994

ABSTRACT

Continuous periodogram analyses of sets of 50 to 364 daily mean atmospheric columnar total ozone content at 19 globally representative stations indicate that the power spectra follow the universal inverse power law form of the statistical normal distribution. The results are consistent with prediction of a cell dynamical system model for atmospheric flows extending up to the stratosphere and above. The unique quantification for nonlinear variability of daily atmospheric total ozone implies predictability of the total pattern of fluctuations.

Key words: Ozone, Columnar total ozone

I. INTRODUCTION

Atmospheric columnar total ozone content exhibits non–linear variability on all time scales from days to years. A major portion of the total ozone resides as a thin layer in the stratosphere and plays the very important role of absorbing solar ultraviolet radiation which is harmful for life on earth. It is important to identify and quantify the physics of the total pattern of fluctuations for predictability studies. Earlier studies have shown that total ozone exhibits short term periodicities of about 2–3 days, 5–6 days, 10–15 days, 30–40 days etc. Such periodicities have been associated with wave activity in the middle atmosphere (Maruyama, 1991). In the present study, it is shown that continuous periodogram analyses of 22 sets of 50 to 364 days total ozone at 19 globally representative stations follow the universal inverse power law form of the statistical normal distribution. Inverse power law forms for power spectra indicating long–range temporal correlations (persistence) are ubiquitous to real world dynamical systems, in particular geophysical parameters (Agnew, 1992) and are now identified as signatures of self–organized criticality (Bak, Tang and Wiesenfeld, 1988). The physics of self–organized criticality is not yet identified. The results presented in this paper are in agreement with a recently developed cell dynamical system model for atmospheric flows (Mary Selvam, 1990; Mary Selvam et al., 1992; Mary Selvam, 1993) which predicts inverse power law form of the statistical normal distribution for the power spectra as a natural consequence of quantum–like mechanics governing flow dynamics. Such unique quantification for self–organized criticality implies predictability of the total pattern of fluctuations in total ozone.

II. CELL DYNAMICAL SYSTEM MODEL

In summary (Mary Selvam, 1990; Mary Selvam et al., 1992) the model is based on the concept of Townsend (1956) that large eddy structures form in turbulent shear flows as the spatial integration of enclosed turbulent eddies. Therefore, the energy (kinetic) of

progressively larger eddies follow the normal distribution characteristics according to the Central Limit Theorem in Statistics. The square of the eddy amplitude will then represent the probability of occurrence of eddy fluctuations. Similar laws govern the subatomic dynamics of quantum systems (Maddox, 1988). Atmospheric flows therefore follow quantum–like mechanical laws as a natural consequence of Townsend's concept of the physics of large eddy growth in turbulent shear flows stated above. Further, the model predicts an overall logarithmic spiral trajectory for atmospheric flows with the quasiperiodic Penrose tiling pattern for the internal structure. The quantitative model predicted governing equations are given in the following.

The logarithmic wind profile relationship is given as

$$W = \frac{w_*}{\mathbf{k}} \log Z \ , \tag{1}$$

where W and w_* are the root mean square (r.m.s) circulation speeds of eddies of respective radii R and r, with length scale ratio Z equal to R/r. The von Karman's constant $\mathbf{k}$ is equal to $1/\tau^2$ where τ is the golden mean $[=(1+\sqrt{5})/2=1.618]$ and represents the fractional volume dilution of large eddy by enclosed turbulent eddy fluctuations and consequent mixing with environment.

The r.m.s. circulation speed W at each stage forms the mean level for the next stage of large eddy growth. Therefore W represents the standard deviation of the eddy fluctuations at each stage and also the mean for the next stage of eddy growth. The logarithm of the length (and therefore the time) scale ratio Z represents the standard deviation of the eddy fluctuations (Eq.1). Therefore if L represents the period,

$$\log L \ \alpha \ W. \tag{2}$$

The conventional power spectrum plotted as the percentage contribution to total variance versus the period in log–log scale will now represent the eddy probability on logarithmic scale versus the standard deviation of the eddy fluctuations on linear scale. Since the r.m.s. eddy fluctuation W probabilities follow normal distribution characteristics because of quantum–like mechanics governing flow dynamics, normalized standard deviation t can now be defined as

$$t = \frac{\log L}{\log T_{50}} - 1 \ , \tag{3}$$

where L is the period and T_{50} the period up to which the cumulative percentage contribution to total variance is equal to 50. t as derived above corresponds to the normal variate in conventional statistics defined as

$$t = \frac{X - \overline{X}}{\sigma} \ ,$$

where $\overline{X}$ and σ are the mean and standard deviation of the variable X which is distributed normally. The mean $\overline{X}$ corresponds to cumulative percentage probability of occurrence equal to 50. In the present study $\log L$ represents the variable X and $\log T_{50}$ represents the mean $\overline{X}$ and also the standard deviation σ of the distribution of r.m.s. eddy fluctuation W as explained above (Eqs.1 and 2).

The power spectrum when plotted as cumulative percentage contribution to total variance versus the t values (Eq.3) will represent the statistical normal distribution.

The signatures of the model predicted logarithmic spiral flow structure will be seen in conventional power spectra of meteorological parameters as a continuum of eddies with a

smooth rotation of phase angle concomitant with increasing period length. The model predicted quasiperiodic Penrose tiling pattern for the internal flow structure will be seen in the eddy continuum as embedded dominant wavebands, the bandwidth increasing with period length. The peak period L_n for the nth waveband is given as

$$L_n = \tau^n (2+\tau)t \ , \tag{4}$$

where n ranges from negative to positive integer values including zero and t is the solar powered primary perturbation time period. t refers to the diurnal cycle of solar heating for the daily total ozone time series used in the present study.

Continuous periodogram analyses of daily total ozone content at globally representative stations are in agreement with model predictions as shown in the following section.

III. DATA AND ANALYSIS

Daily values of atmospheric total ozone for 19 globally representative stations were obtained from OZONE DATA FOR THE WORLD (1987–1991). Continuous periodogram analyses (Jenkinson, 1977) were done for 22 sets of 50 to 364 daily maen total ozone time series. The broadband power spectrum of total ozone time series can be computed accurately by the elementary but powerful method of analysis developed by Jenkinson (1977) which provides a quasi–continuous form of classical periodogram allowing systematic allocation of total variance and degrees of freedom of the data series to logarithmically spaced elements of the frequency range (0.5,0). The periodogram is constructed for a fixed set of 10000 (m) periodicities which increase geometrically as $L_m = 2\exp(Cm)$ where $C = .001$ and $m = 0,1,2,\cdots$ m. The data Y_t for the N data points were used. The periodogram estimates the set of $A_m \cos(2\pi t_m - \varphi_m)$ where A_m, t_m and φ_m denote respectively the amplitude, frequency and phase angle for the mth period. The cumulative percentage contribution to total variance was computed from high frequency side of the spectrum. The period T_{50} at which 50% contribution to total variance occurs is taken as reference and the normalized standard deviation t_m values are computed as (Eq.3)

$$t_m = (\log L_m / \log T_{50}) - 1 \ .$$

The spectra as determined by continuous periodogram analyses are plotted in Fig. 1 as cumulative percentage contribution to total variance versus the normalized standard deviation t. The statistical normal distribution is also plotted as crosses in Fig. 1 and represent the cumulative percentage probability for the normalized standard deviation t. The power spectra follow the normal distribution characteristics as determined by the statistical chi–square test for "goodness of fit" at 95% confidence level (Spiegel, 1961). Table 1 gives the mean and standard deviation of the data, the periodicities T_{50}, T_{75}, T_{90} up to which the cumulative percentage contribution to total variance is equal to 50, 75, 90 respectively and the peak periodicities for dominant wavebands for which the normalized variance is equal to or greater than 1.

The fine structure characteristics of variance and phase are shown in Fig. 2 for a representative periodogram. It is seen that the spectrum is broadband with embedded dominant eddies, the bandwidth increasing with period length. Further, there is a continuous smooth rotation of phase angle concomitant with increase in period within a waveband and from one waveband to the next implying spiral–like flow structure in the stratosphere and are consistent with model predictions (see Section II).

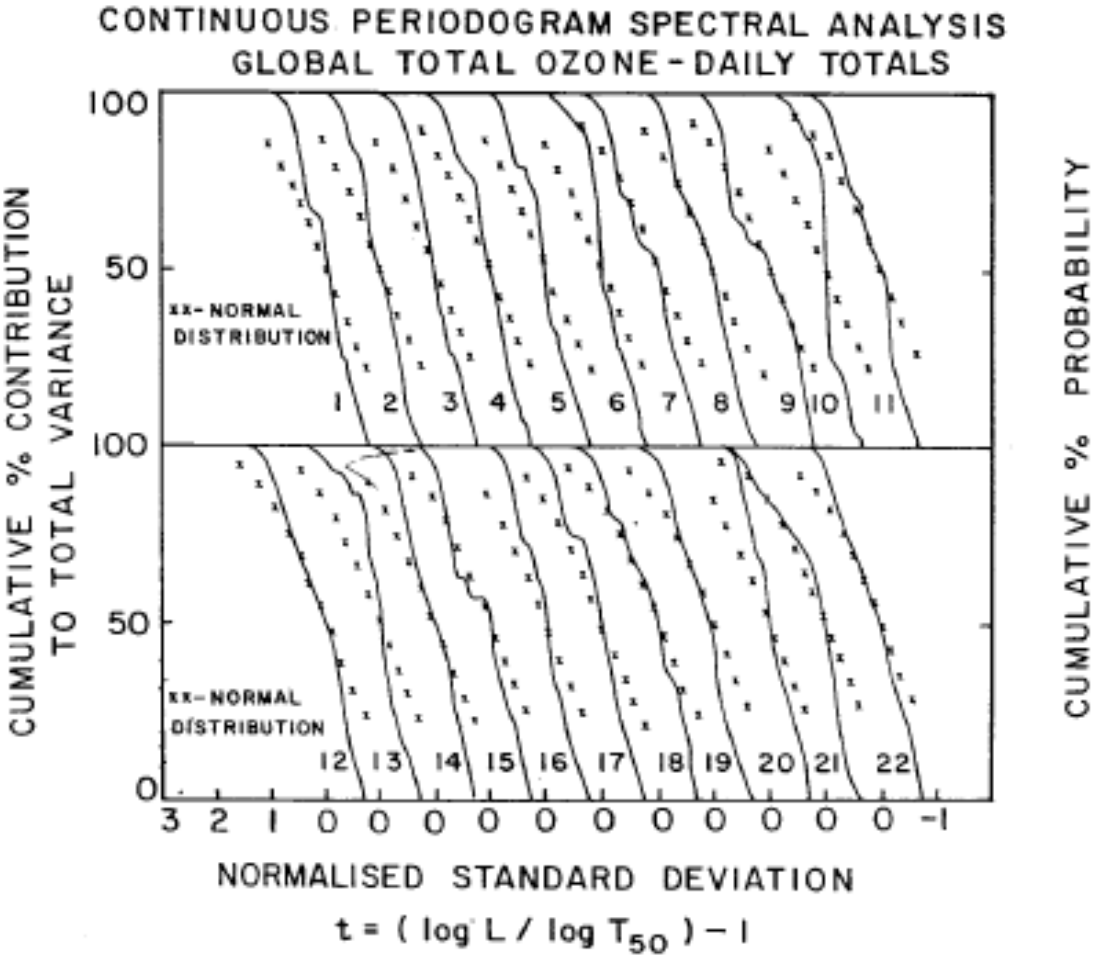

Fig. 1. Continuous periodogram spectral analyses of daily atmospheric columnar total ozone for 22 sets of time series data listed in Table 1.

IV. DISCUSSION AND CONCLUSION

The spectra of temporal (days) fluctuations of atmospheric columnar total ozone follow the universal and unique inverse power law form of the statistical normal distribution. Inverse power law form for power spectra indicates long–range temporal correlations (persistence) and is a signature of self–organized criticality in the day to day fluctuations of total ozone.

The results are consistent with the cell dynamical system model prediction of such a universal spectrum for self–organized criticality in atmospheric flows as a natural consequence of quantum–like mechanics governing flow dynamics. The unique quantification for self– organized criticality implies predictability of the total pattern of fluctuations in the atmospheric total columnar ozone over a period of time. It may therefore be possible to predict future trends in atmospheric total columnar ozone content. The applications of the above result for predictability studies will be presented in a separate paper.

The peak periodicities in the wavebands with normalized variance equal to or more than 1 (Table 1) correspond to the time periods of the quasiperiodic Penrose tiling pattern traced by internal circulations of the large eddy (see Section II) and are respectively equal to $(2/\tau + 1)t = 2.2t$, $(2 + \tau)t = 3.6t$, $\tau(2 + \tau)t = 5.8t$, $\tau^2(2 + \tau)t = 9.5t$, $\tau^3(2 + \tau)t = 15.3t$, $\tau^4(2 + \tau)t = 24.8t$, $\tau^5(2 + \tau)t = 40.1t$ where t, the primary perturbation time period, is the diurnal cycle of solar heating. The dominant periodicities in atmospheric columnar total ozone time series may therfore be expressed as functions of the golden mean. Other studies of total ozone variability (Chandra, 1986; Gao and Stanford, 1990; Prata, 1990; Dunkerton, 1991) also show quasiperiodicities close to those predicted above.

Table 1. Periodogram Estimates for Total Ozone

Sr. No.	Station (Lat Long) (Degrees)	Time series length (Days)	Period From	To	Mean	Std. Dev.	T 50	T 75	T 90	Periodicities (days) contributing to maximum normalized variance (H) in the wave band H > = 1					
					m atm-cm			(Days)								
1.	Pechora (65.07N, 57.96E)	75	1 Apr. 88	14 Jun. 88	426.6	48.4	21.6	79.4	128.5	6.4	9.9	16.0	23.2	37.3	–
2.	Voronez* (51.40N, 39.35E)	100	1 Mar. 88	8 Jul. 88	393.5	37.6	22.7	59.7	149.2	5.1	5.6	6.1	6.5	7.9	9.7
										11.0	14.6	23.6	32.9	56.2	–
3.	Semipalatinsk (50.2N, 80.15E)	50	1 Apr. 87	20 May. 87	398.7	35.4	10.3	24.4	44.4	2.0	2.7	4.0	7.3	9.1	25.3
4.	Bismarck* (46.49N, 100.5E)	120	1 Jul. 89	28 Oct. 89	304.7	18.8	17.4	38.4	145.6	5.2	7.1	8.3	11.6	17.9	29.8
5.	Cardzou* (39.10N, 63.30E)	235	1 Apr. 88	21 Nov. 88	301.2	24.4	31.7	89.6	349.4	3.3	3.9	6.3	7.3	7.6	8.7
										9.1	11.7	13.0	14.3	15.5	21.1
										23.5	29.9	49.0	–	–	–
6.	Dushanbe (38.35N, 68.47E)	180	1 Apr. 88	27 Sep. 88	303.4	25.8	28.0	45.1	131.5	2.8	3.1	3.3	4.0	4.8	5.7
										6.9	7.6	11.3	12.8	14.9	21.2
										29.2	49.2	–	–	–	–
7.	Tateno* (36.03N, 140.08E)	100	1 May 90	8 Aug. 90	323.0	25.4	15.3	102.7	173.5	4.7	6.0	7.7	8.5	9.3	11.0
										14.9	20.7	–	–	–	–
8.	Cairo* (30.02N, 31.15E)	364	1 Jan. 89	31 Dec. 89	302.3	17.1	29.1	321.6	549.0	5.8	5.9	6.0	6.9	7.0	7.3
										7.8	8.0	8.3	8.5	8.9	9.4
										9.7	9.9	10.2	10.6	10.9	12.0
										12.6	14.8	17.2	19.8	25.2	29.9
										37.1	42.1	49.6	60.0	97.4	162.1
9.	Cairo	180	1 Jun. 88	27 Nov. 88	292.0	16.1	19.6	203.8	328.4	2.0	2.3	2.5	2.6	2.9	3.0
										3.2	3.7	3.8	3.9	4.1	4.3
										5.4	5.6	6.2	6.5	8.8	9.4
										15.6	17.5	19.7	22.5	26.2	31.3

Continued **Table 1.** Periodogram Estimates for Total Ozone

10. Varanasi (25.2N, 83.0E)	50	1	Apr.	91–20	May	91	296.7	9.4	13.3	17.5	39.6	4.6	5.2	13.1	49.2	–	–
11. Aswan (24.05N, 32.57E)	75	1	Jun.	89–14	Aug.	89	300.9	5.8	10.1	40.3	72.9	4.9	5.3	5.9	6.7	8.8	15.4
												21.0	65.3	–	–	–	–
12. Poona* (18.32N, 73.51E)	75	1	Jan.	88–16	Mar.	88	252.2	9.1	10.1	47.2	91.3	2.3	3.5	3.9	4.4	4.7	5.4
												5.8	6.4	7.0	7.8	8.8	10.2
												14.0	17.7	27.6	–	–	–
13. Reykjavik (64.00N, 21.30W)	120	1	Mar.	91–28	Jun.	91	394.2	36.2	12.8	22.5	85.9	2.8	3.2	5.9	6.8	7.3	9.1
												12.1	21.6	32.3	105.1	–	–
14. Reykjavik (53.35N, 21.30W)	75	1	Jul.	88–13	Sep.	88	333.6	29.9	14.3	53.4	91.9	3.4	3.7	4.4	5.2	5.7	6.9
												7.7	9.9	11.4	17.0	–	–
15. Goose (53.19N, 60.23W)	75	15	May	87–28	Jul.	87	368.0	27.6	12.93	84.1	133.1	2.3	3.1	3.4	4.0	5.8	7.7
												8.8	10.2	12.4	16.1	35.4	–
16. Fresno* (36.50N, 120.50W)	50	1	Aug.	89–19	Sep.	89	309.9	11.0	10.0	19.2	35.6	2.0	4.3	5.1	6.0	8.0	16.6
17. Fresno	120	1	May	88–28	Aug.	88	328.4	26.7	17.8	85.2	198.0	6.1	7.8	9.6	10.6	16.5	20.0
												24.6	44.0	–	–	–	–
18. Hobart* (42.53S, 147.21E)	100	1	Mar.	88–8	Jun.	88	278.9	13.8	10.9	43.6	116.4	2.2	2.4	2.8	2.9	3.2	3.5
												4.4	5.2	7.8	8.7	9.8	11.2
												19.6	40.9	–	–	–	–
19. Melbourne* (37.5S, 144.59E)	50	1	Oct.	90–19	Nov.	90	326.2	24.2	10.1	43.7	74.2	4.9	9.7	62.7	–	–	–
20. Perth* (32.00S, 115.57E)	75	1	Apr.	90–14	Jun.	90	278.2	12.9	11.8	26.1	41.2	2.1	2.4	2.8	6.5	7.5	8.5
												9.9	11.5	14.3	37.6	–	–
21. Brisbane (27.30S, 153.00E)	120	1	Jul.	88–28	Oct.	88	307.3	20.6	9.2	32.3	145.9	3.7	4.3	4.7	5.5	5.9	7.0
												8.8	14.3	18.3	27.9	–	–
22. Nairobi (01.18S, 36.52E)	210	1	Nov.	88–29	May	89	251.6	10.7	15.9	83.2	220.6	8.6	11.8	19.1	32.5	–	–

std. dev.: standard deviation of the time series.

* denotes that the data series is not distributed normally.

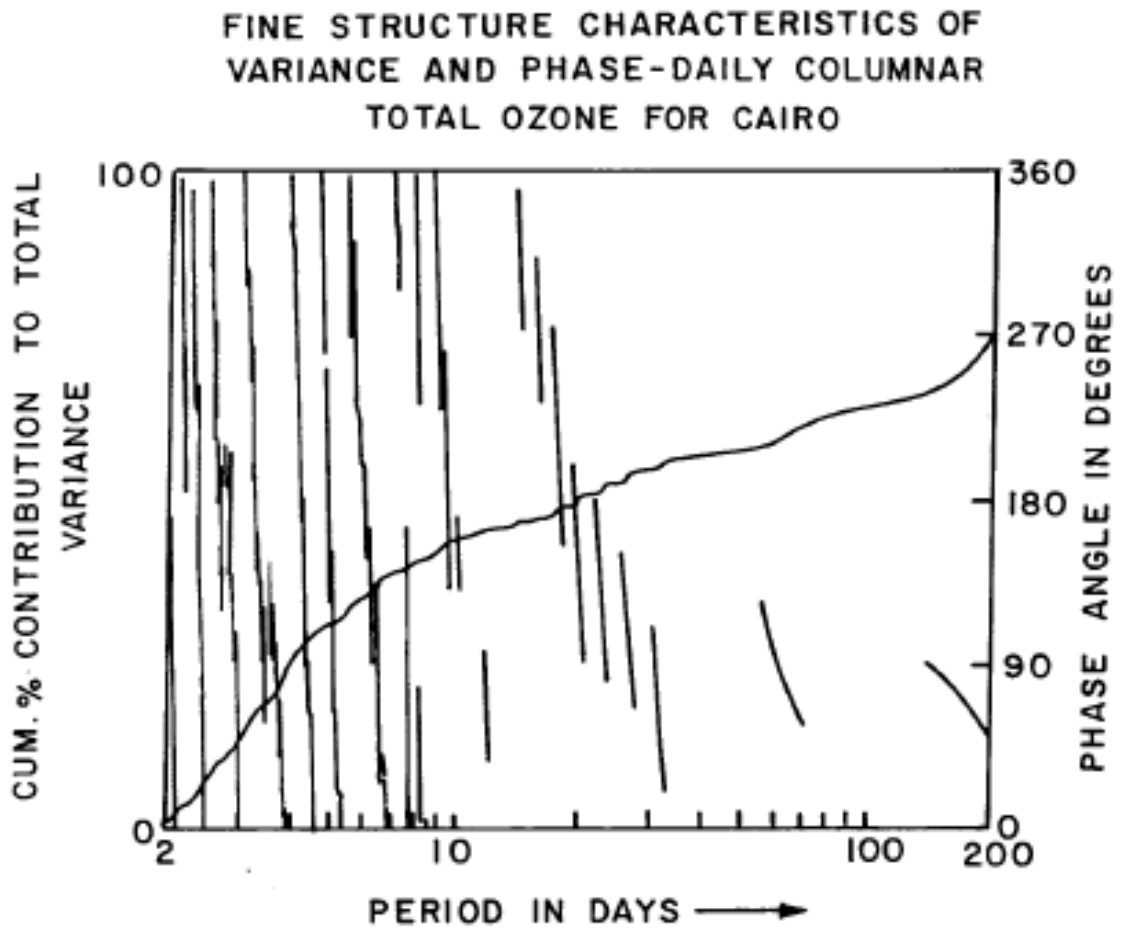

Fig. 2. Fine structure characteristics of variance and phase in the continuous periodogram analyses of atmospheric columnar total ozone at Cairo for a set of 180 days (1 Jun–27 Nov.88). The cumulative percentage contribution to total variance is plotted as a continuous line. The phase angle for dominant periodicities with percentage contribution to total variance exceeding 0.01 alone is plotted as continuous lines.

The authors are grateful to Dr. A. S. R. Murty for his keen interest and encouragement during the course of this study. Thanks are due to Mr. M. I. R. Tinmaker for typing the manuscript.

REFERENCES

Agnew, D.C. (1992), The time–domain behaviour of power–law noises, *Geophys. Res. Lett.*, **19(4)**: 333–336.

Bak, P.C., Tang, C. and Wiesenfeld, K. (1988), Self–organized criticality, *Phys.Rev.* **A38**: 364–374.

Chandra, S. (1986), The solar and dynamically induced oscillations in the stratosphere, *J.Geophys.Res.*, **91(D2)**: 2719–2734.

Dunkerton, T.J. (1991), LIMS (Limb Infrared Monitor of the Stratosphere) Observation of travelling planetary waves and potential vorticity advection in the stratosphere and mesosphere, *J.Geophys.Res.*, **96(D2)**: 2813–2834.

Gao, X.H. and Stanford, J.L. (1990), Low frequency oscillations in total ozone measurements, *J.Geophys.Res.*, **95(D9)**: 13797–13806.

Jenkinson, A.F. (1977), A powerful elementary method of spectral analysis for use with monthly, seasonal or annual meteorological time series, Met. 0 13 Branch Memorandum No.57, pp.22.

Maddox, J. (1988), Licence to slang Copenhagen? *Nature*, **332**: 581.

Maruyama T. (1991), Annual and QBO-synchronized variations of lower-stratosphere equatorial wave activity during 1961-1989, *J.Met.Soc.Japan*, **69:** 219-232.

Mary Selvam, A. (1990), Deterministic chaos, fractals and quantum-like mechanics in atmospheric flows, *Can.J.Phy.*, **68:** 831-841.

Mary Selvam, A., Pethkar, J.S., and Kulkarni, M.K. (1992), Signatures of a universal spectrum for atmospheric interannual variability in rainfall time series over the Indian region. *Int'l.J.Climatol.*, **12(2):** 137-152.

Mary Selvam, A. (1993), A universal spectrum for interannual variability of monsoon rainfall over India, *Adv.Atmos.Sci.*, **10(2):** 221-226.

Ozone data for the world (1987-1991), Atmospheric Environment Service, Environment Canada.

Prata, A.J. (1990), Travelling waves in Nimbus-7 SBUV Ozone measurements: Observations and theory, *Quart.J.Roy.Meteorl.Soc.*, **116(B):** 1091-1122.

Spiegel, M.R. (1961), Statistics, Schaum's outline series, McGraw-Hill Book Co., New York.

Townsend, A.A. (1956), *The structure of turbulent shear flow*, Cambridge University Press, U.K.